Physisorption-Induced Structural Change Directing Carbon Monoxide Chemisorption and Nitric Oxide Coordination on Hemilabile Porous Metal Organic Framework $NaNi_3(OH)(SIP)_2(H_2O)_5 \cdot H_2O$ (SIP = 5-sulfoisophthalate)

Jon. G. Bell[1], Samuel A. Morris[2], Farida. Aidoudi[2], Laura J. McCormick[2,3], Russell E. Morris[2], K. Mark. Thomas[1]

[1]Wolfson Northern Carbon Reduction Laboratories, School of Chemical Engineering and Advanced Materials, Newcastle University, Newcastle upon Tyne, NE1 7RU, U.K.

[2]School of Chemistry, Purdie Building, St Andrews University, North Haugh, St Andrews, Fife KY16 9ST, U.K.

[3]Experimental Systems Group, Advanced Light Source, Berkeley, California, USA

Abstract

Structural changes occur during the thermal activation of $NaNi_3(OH)(SIP)_2(H_2O)_5 \cdot H_2O$ and $NaCo_3(OH)(SIP)_2(H_2O)_5 \cdot H_2O$ to form porous framework materials. Activation at 400K gave $NaNi_3(OH)(SIP)_2(H_2O)_2$ and 513K gave $NaNi_3(OH)(SIP)_2$. CO adsorption/desorption on $NaNi_3(OH)(SIP)_2(H_2O)_2$ at 348K and 20 bar was hysteretic, but all CO was desorbed in vacuum. $NaNi_3(OH)(SIP)_2(H_2O)_2$ was exposed to NO to establish the accessibility of unsaturated metal centers and crystallographic results show that NO binds to Ni with bent coordination geometry. The adsorption characteristics of CO on isostructural $NaNi_3(OH)(SIP)_2$ and $NaCo_3(OH)(SIP)_2$ were studied over the temperature range 268–348K and pressures up to 20bar. CO surface excess isotherms for $NaNi_3(OH)(SIP)_2$ at 348K were reversible and non-hysteretic for pressures below the isotherm point of inflection. However, above this point, isotherms had both reversible and irreversible adsorption components. The irreversible component remaining adsorbed in ultra-high vacuum at 348K was 4.9 wt%. Subsequent sequential CO adsorption/desorption isotherms were non-hysteretic and fully reversible. The thermal stability and stoichiometry of the product were investigated by *in-situ* temperature programmed desorption combined with thermogravimetric analysis and mass spectrometry. This gave a discrete CO peak at ~500K indicating thermally stable bonding of CO to the framework (0.42×CO per formula desorbed (2.31 wt%)) and a weaker CO_2 peak was observed at 615K. The remaining adsorbed species were desorbed as a mixture of CO and CO_2 overlapping with $NaNi_3(OH)(SIP)_2$ framework decomposition. CO physisorption induces structural change, which leads to CO chemisorption on $NaNi_3(OH)(SIP)_2$ above the point of inflection in the isotherm, with the formation of a new thermally stable porous framework. The porous structure of the framework was confirmed by CO_2 adsorption at 273K. Therefore, CO chemisorption is attributed to breaking of the hemilabile switchable sulfonate group, while the framework structural integrity is retained by the stable carboxylate linkers. In contrast, studies of CO adsorption on $NaCo_3(OH)(SIP)_2$ showed hysteretic isotherms, but no evidence for irreversible chemisorption CO was observed. The CO/N_2 selectivity for $NaNi_3(OH)(SIP)_2$ and $NaCo_3(OH)(SIP)_2$ were 2.4–2.85(1–10 bar) and 1.74–1.81(1–10 bar). This is the first demonstration of physisorption driving structural change in a hemilabile porous framework material and demonstrates a transition from physisorption to irreversible thermally stable CO chemisorption.

1. INTRODUCTION

Metal organic framework materials (MOFs) are porous materials with versatile surface chemistry with potential for post synthetic modification and may have framework flexibility. This wide ranging surface chemistry and functionality gives rise to interesting potential applications of these porous solids ranging from gas storage[1-3], separation[4, 5], purification[6, 7], catalysis[8, 9], drug delivery[10], and sensing extending to biology and medicine[10, 11]. New developments depend on developing novel and unusual chemical approaches to the design of the MOF materials. In the case where a linker has two types of coordinating group, one of which binds strongly to a metal, while the other binds more weakly, it will lead to the possibility of 'hemilabile' MOFs where the strongly bound groups hold the MOF together, while interesting chemistry can take place at the more weakly bound group, making and breaking the weak bonds. This concept has previously been demonstrated using a copper 5-sulfoisophthalate material. The 5-sulfoisophthalate linker has two carboxylates (which bind strongly to copper) and one sulfonate group (which binds more weakly to copper).[12] The important feature of this material is that on activation (desolvation) the metal carboxylate framework remains intact, while the coordination at the sulfonate can undergo a reversible change. We have shown that this is a single crystal to single crystal transformation (although, the crystal goes through a disordered state before the ordered state returns). These MOFs are described as hemilabile by analogy with ligands that are used in molecular coordination chemistry and homogenous catalysis. The hemilability of the MOFs opens the possibility of unusual properties, and Cu-SIP-3 shows ultra-selective adsorption towards gases that coordinate strongly to metals, such as nitric oxide, leading to potential impact in both sensing and medical materials, and also in catalytic applications. Switchable pore-discriminating adsorption properties have also been shown to exist in a hydrophilic/hydrophobic metal organic framework[13].

Carbon monoxide is produced in many industrial processes, for example, integrated gasification combined cycle for syngas production and is used commercially in the manufacture of methanol, acetic acid etc. Separation of CO from N_2 is very difficult due to the similar physical properties.[14] The adsorption characteristics of CO are important in the context of separation of $CO_2/CH_4/CO$ mixtures in pressure swing adsorption.[15] Gas separation is a very energy intensive process and the development of new adsorbents for CO adsorption is an important area of research with possible applications in gas separation and purification.[16] Carbon monoxide is also a very toxic gas, which binds strongly with hemoglobin and must be removed from compressed air for breathing, respirators etc. In porous materials, the greatest

variety of potentially strongly interacting sites for CO adsorption exists in MOFs. However, comparison of dynamic adsorption breakthrough studies eight toxic gases/vapors (SO_2, NH_3, Cl_2, C_6H_6, CH_2Cl_2, C_4H_8S, C_2H_4O and CO) on a range of MOFs (MOF-5,IRMOF-3, IRMOF-62, MOF-74, MOF-177 and MOF-199) and BPL carbon showed that CO was not captured effectively by any of the adsorbents studied due to only relatively weak interactions, whereas the other gases/vapors were captured.[17] Recent research has shown that MOFs can reversibly adsorb relatively large quantities of carbon monoxide through reversible interaction with open metal centers at low temperatures.[18] The enthalpies of adsorption for CO were in the range 19-53 kJ mol^{-1} for temperatures in the range 77-318 K.[18-20] CO is known to coordinate with metals but there is currently only evidence for weak interactions with metals in MOFs.

The use of MOFs with hemilabile and switchable coordination chemistry represents a new development in materials.[21, 22] A key feature of understanding the adsorption processes occurring in both hemilabile and switchable MOFs relates to structural change in response to a chemical stimulus in the form of small molecules.[21, 22] The aim of this study was to investigate the influence of surface and structural chemistry in facilitating structural change in a framework with hemilabile coordination chemistry, which could facilitate CO and NO adsorption by coordination to the metal. The adsorption of isoelectronic CO and N_2 on iso-structural metal organic frameworks $NaNi_3(OH)(SIP)_2$ and $NaCo_3(OH)(SIP)_2$, where SIP = 5-sulfoisophthalate, were also compared. The surface chemistry in $NaNi_3(OH)(SIP)_2$ and $NaCo_3(OH)(SIP)_2$ includes sodium ions, acidic OH groups, unsaturated metal centers and also, hemilabile sulfonate group coordination to the metal. The interaction of CO with the sodium cations, acidic OH functional groups and unsaturated metal centers can enhance adsorption. Initially, reversible physisorption occurs, influenced by synergistic surface chemistry with confinement in pores. At a well-defined loading, a structural change occurs to form a reactive structure in the case $NaNi_3(OH)(SIP)_2$, which irreversibly chemisorbs CO with the formation of a new porous structure on which CO is immobilized and further physisorption occurs. As far as we are aware, this is the first observation of this mechanism for the chemisorption of CO on a porous material. The adsorption results are discussed in terms of structural change, thermodynamics, kinetics and switchable hemilabile coordination. Hemilabile and switchable MOF materials may have applications in gas separation and purification and, in this particular case, the removal of trace amounts of CO from air, as well as CO storage under low system pressure.

2. EXPERIMENTAL

2.1 Synthesis of $NaNi_3(OH)(SIP)_2(H_2O)_5{\cdot}H_2O$ and $NaCo_3(OH)(SIP)_2(H_2O)_5{\cdot}H_2O$

$Ni(OH)_2$ (Sigma Aldrich, 2 g (21.7 mmol) and the mono sodium salt of 5-sulfoisophthalic acid "NaH_2SIP" (TCI, 2.916 g (10.9 mmol) were mixed in a mortar, then 1 mL of HCl (37% in water) was added dropwise with continuous mixing. The paste-like mixture was then transferred into a Teflon vessel and sealed inside a stainless steel autoclave, and heated to 453 K for 48 h. The autoclave was cooled down to room temperature A green crystalline product was obtained, which was sonicated in 100 mL of water, filtered, and washed three times with water to remove any unreacted NaH_2SIP. The final green powder was air-dried was $NaNi_3(OH)(SIP)_2(H_2O)_5{\cdot}H_2O$. $NaCo_3(OH)(SIP)_2$ was obtained following an analogous procedure, reacting $Co(OH)_2$ with the mono sodium salt of 5-sulfoisophthalic acid. A purple crystalline product was produced.

2.2 Single Crystal X-ray Diffraction Studies on Partially Dehydrated Samples

A rod-like green crystal with dimensions of 0.018 × 0.009 × 0.076 mm was chosen and mounted on the single crystal X-ray diffractometer at the Advanced Light Source (ALS), Berkeley, California, US. A wavelength of 0.77490 Å was used throughout all collections. Further details are in the crystallographic information files (CIFs).

The $NaNi_3(OH)(SIP)_2(H_2O)_5{\cdot}H_2O$ crystal was held inside a gas cell under ambient conditions and the first data set collected under ambient conditions. A dynamic vacuum was applied in step-wise increments down to ≈ 6 mTorr. The sample was heated at 100 K h^{-1} to 400 K using a nitrogen blower and left to equilibrate for one hour before the next data set was collected (400K-1). To expose the cell to carbon monoxide, a three-stage valve system was used. A combination of CO and dynamic vacuum was used to ensure the lines were purged of any residual gases prior to loading into the cell. The sample was exposed to carbon monoxide at a pressure of ≈ 800 Torr and left to equilibrate for one hour (400K-CO). The crystal was re-activated through elevation at 100 K h^{-1} to 400 K and was held for one hour (400K-2). The crystal was subsequently exposed to ≈ 790 Torr of NO and left to equilibrate for one hour (400K-NO). Finally, the crystal was returned to room temperature and opened to the atmosphere (RT-2) Attempts to dehydrate the single crystals at 500 K were unsuccessful, leading to loss of diffraction from the single crystals on the diffractometer.

Crystal structures were solved using SHELXT[23] and all framework atoms assigned with the exception of water molecules. Least squares refinements of the model were carried out using SHELXL. Water molecules were first assigned at full occupancy and a thermal parameter of 0.05 $Å^2$, which was allowed to freely refine; if significant deviations occurred their occupancy was refined. If the water was disordered over multiple positions, their occupancies were linked and refined as a free variable, with their thermal parameters of 0.05 $Å^2$ set until their occupancies stabilised, then freely refined. Aromatic hydrogens were placed geometrically, while water hydrogens were only assigned if strong enough electron density was observed, upon which they were fixed at 0.9 Å from their parent oxygen and 1.47 Å from each other – ensuring a H-O-H angle of 109.5 °. All framework atoms were refined anisotropically unless stated in further discussion. Solvent and gas molecules were refined anisotropically on a per atom basis.

2.3 Powder X-ray Diffraction (PXRD) studies

PXRD profiles were collected at the Diamond Light Source in Oxfordshire, U.K., on beamline I11. The samples were ground and packed into 0.5 mm outer diameter borosilicate capillary tubes and dehydrated, if required, using a Buchi glass oven held at 573 K under high vacuum overnight. The samples were then rapidly removed and flame-sealed to minimize exposure to the atmosphere. On the beamline, the samples were spun and illuminated using a monochromatic beam with a wavelength of 0.826048 Å. The samples had a zero point error of -0.0312 ° as determined by a silicon standard. The Mythen II PSD detector was used for data collection that occurred for two 10 s scans from 2.25 – 90° 2θ, which were summed together to improve the statistics. Data was refined using TOPAS Academic ver.5 with all refinements carried out from 3 – 38 ° 2θ, with the region 8.17 – 8.5 ° 2θ excluded due to an impurity peak.

2.4 Gas Adsorption Studies

Adsorption characteristics of carbon monoxide, nitrogen and carbon dioxide on $NaNi_3(OH)(SIP)_2$, $NaNi_3(OH)(SIP)_2(H_2O)_2$ and $NaCo_3(OH)(SIP)_2$ were investigated using an Intelligent Gravimetric Analyzer (IGA), supplied by Hiden Isochema Ltd., Warrington, UK. The system is an ultra-high vacuum (UHV) system comprising of a fully computer controlled microbalance with a weighing resolution of 0.2 μg and long-term stability of ± 1 μg. The pressure and temperature regulation were computer controlled. The pressure transducers had individual ranges of 0–0.2 kPa, 0–10 kPa and 0–2000 kPa. Trace amounts of gas contaminants were removed from the IGA inlet gas stream using 13X zeolite for drying and activated carbon

for removal volatile organic compounds. The adsorbent purification system was heated to 773 K for two days under ultra-high vacuum between each experiment to regenerate the adsorbent bed. An additional zeolite *in situ* drying system was used to remove trace amounts of water vapor from within the IGA system. This system was also heated to 773 K under ultra-high vacuum between adsorption experiments.

The $NaNi_3(OH)(SIP)_2\ (H_2O)_5{\cdot}H_2O$ sample (50 ± 1 mg) was outgassed to a constant weight, at < 10^{-6} Pa, at either 403 K or 513 K, which corresponded to the removal of 4 and 6 water molecules per crystallographic formula unit from the porous structure, respectively (as shown in Figure S1). $NaCo_3(OH)(SIP)_2(H_2O)_5$ was outgassed at 448 K, which corresponds to the final plateau in the thermogravimetric profile. Repeatability measurements for CO adsorption isotherms at 348 K for loading experiments are shown in Figure S6. The standard deviation for repeatability at 10 bar was ± 1.27% of the surface excess value. The equilibrium uptake value was determined as being 99 % of the predicted value, calculated in real time using the mass uptake profile. Saturated vapor pressures were calculated using the Antoine equation:

$$\log p^0 = A - \frac{B}{T + C} \tag{1}$$

where p^0 is the saturated vapor pressure (Torr), T is the temperature (K), and A, B, and C are adsorbate dependent constants. The parameters used for each adsorptive are as follows: nitrogen (-200 to -147ºC) (A) 6.49457, (B) 255.68, (C) 266.55[24]; carbon dioxide (-196 to 30°C) (A) 7.81024, (B) 995.705, (C) 293.475. [25]

2.5 Temperature Programmed Desorption (TPD)

2.5.1 Activation and Thermal Stability Studies

Thermogravimetric analysis (Thermal Sciences STA 1500 thermogravimetric analyzer) and mass spectrometry (VG Quadrupoles 300 amu) was used to investigate the loss of water during the activation procedure and the decomposition of the MOFs. The thermogravimetric characteristics and the evolved gases were monitored as a function of temperature during pyrolysis at 10 K min^{-1} in a flow of helium (60 cm^3 min^{-1}). The sampling probe inlet, which comprised of a l mm diameter stainless steel tube lined with a deactivated fused silica capillary was located ~ 1 cm above the sample. This allows the detection of both stable decomposition products and reactive intermediate species.[26] Mass/charge (m/z) ratios of 18(H_2O), 28(CO), 32

(O_2), 44(CO_2) and 64(SO_2), weight loss and sample temperature were monitored simultaneously throughout the TPD experiments.

2.5.2 In-Situ Temperature Programmed Desorption of Adsorbed CO

Sequential Isotherm Studies

In-Situ TPD thermogravimetric measurements in UHV were carried out after the sequential adsorption/desorption experiments in the IGA to confirm the amount of chemisorbed CO retained on the sample. Measurements on samples after sequential CO adsorption /desorption cycles at 348 K for $NaNi_3(OH)(SIP)_2(CO)_x$ up to 20 bar were carried out at heating rates of 1 K min^{-1}.

CO Treatment Studies

$NaNi_3(OH)(SIP)_2$ was reacted with CO under the maximum pressure and temperature conditions used in the isotherm studies to facilitate a more rapid analysis of the desorbed products with greater accuracy by CO desorption immediately after treatment rather than going through the time consuming desorption isotherm. Mass spectrometry was not sufficiently sensitive under UHV to provide species identification for desorbed products. Therefore Temperature Programmed Desorption combined with Thermogravimetric Analysis coupled with Mass Spectrometry (TG-MS) in flowing helium was performed *in situ* in the IGA system in order to identify the thermal decomposition products of the $NaNi_3(OH)(SIP)_2(CO)_x$ adduct and quantify the weight loss under a helium atmosphere corresponding to the desorbed species. Helium was dried with a zeolite 13X trap, which had been heated and degassed in ultrahigh vacuum (UHV) at 773 K prior to starting the helium flow. The desorbed species were detected using a Hiden Analytical 300 amu quadrupole mass spectrometer connected to the IGA system using a heated gas stainless steel sampling line located 1 cm above the IGA sample bucket. 500 mg of $NaNi_3(OH)(SIP)_2$ sample was initially degassed at 513 K for 4 hours and then exposed to CO at 348 K and 20 bar for two weeks. After the CO exposure period, the IGA system CO pressure was reduced to 1 bar. It was then flushed with dry helium at a flow rate of 50 cm^3 min^{-1} and 1 bar helium pressure to remove any residual CO from the IGA system. The mass spectrometer m/z = 2, 18, 28, 44, 64 peaks were allowed to stabilize under the helium flow. The TPD-MS measurements were then performed at 20 K min^{-1} to increase the sensitivity

by increasing concentration of desorbed species per unit time. The desorbed species and weight loss were monitored as a function of temperature. $NaNi_3(OH)(SIP)_2$ does not contain nitrogen and CO_2 was desorbed at higher temperature, therefore, the m/z = 28 peak is solely desorbed CO.

3. RESULTS

3.1 Activation of $NaNi_3(OH)(SIP)_2(H_2O)_5{\cdot}H_2O$ and $NaCo_3(OH)(SIP)_2(H_2O)_5{\cdot}H_2O$

Temperature programmed differential thermogravimetric analysis showed that both frameworks had two plateaus. The first plateau corresponded to an initial loss of 4 H_2O molecules and the second plateau to loss of a further 2 molecules of H_2O giving a total loss of 6 H_2O molecules (See Figure S1). An activation temperatures of 448 K for $NaCo_3(OH)(SIP)_2(H_2O)_5{\cdot}H_2O$ gave $NaCo_3(OH)(SIP)_2$ while activation temperature of 403 and 513 K for $NaNi_3(OH)(SIP)_2(H_2O)_5{\cdot}H_2O$ gave $NaNi_3(OH)(SIP)_2(H_2O)_2$ and $NaNi_3(OH)(SIP)_2$ respectively. Both $NaNi_3(OH)(SIP)_2(H_2O)_2$ and $NaNi_3(OH)(SIP)_2$ are crystalline and porous. These activation temperatures provide stable framework structures and are well below the framework decomposition temperatures of ~620 K for both $NaCo_3(OH)(SIP)_2$ and $NaNi_3(OH)(SIP)_2$ as shown in the temperature programmed thermogravimetric and mass spectrometry profiles (See Figures S26 and S27).

3.2 Porous Structure Characterization

Adsorption of nitrogen on $NaCo_3(OH)(SIP)_2$ and $NaNi_3(OH)(SIP)_2$ at 77 K gives unrealistically low uptakes due to activated diffusion effects. Figure 1 shows carbon dioxide adsorption isotherms at 195 K. The isotherms are Type I isotherm in the IUPAC classification scheme.[27] The total pore volumes obtained from the CO_2 isotherms was 0.180 $cm^3\ g^{-1}$ and 0.191 $cm^3\ g^{-1}$ for $NaCo_3(OH)(SIP)_2$ and $NaNi_3(OH)(SIP)_2$, respectively. Pore volumes were calculated assuming an adsorbate density of 1.177 g cm^{-3}, which is the CO_2 liquid density at 216.59 K.[28] In comparison, the PLATON pore volumes calculated from crystallographic data for the original hydrated materials were 0.0887 $cm^3\ g^{-1}$ for $NaCo_3(OH)(SIP)_2$ and 0.0949 $cm^3\ g^{-1}$ for $NaNi_3(OH)(SIP)_2$. It is apparent that the total pore volumes obtained from gas adsorption are approximately twice the crystallographic pore volumes. This indicates that the activation process for complete dehydration has led to major structural change with a marked opening of the porous structure. Kim et al reported[29] variable temperature PXRD studies of $NaNi_3(OH)(SIP)_2(H_2O)_5{\cdot}H_2O$ that indicated the onset of porosity at 523 K. Nitrogen adsorption studies on a sample dehydrated at 573 K gave BET and Langmuir surface areas of

750 and 842 m^3 g^{-1}, respectively and a micropore volume of 0.284 cm^3 g^{-1}. These results are consistent with the high total pore volume for $NaNi_3(OH)(SIP)_2$ determined in this study. The high pressure CO_2 isotherm at 273 K for the partially dehydrated $NaNi_3(OH)(SIP)_2(H_2O)_2$ had an isotherm plateau at 2.05 mmol g^{-1} at 20 bar ($p/p^0 \sim 0.57$) (see Figure S11). This corresponds to a pore volume of 0.0874 cm^3 g^{-1} assuming a CO_2 adsorbed phase density of 1.032 g cm^{-3} (CO_2 density at 253 K)[28] , which is similar to the PLATON pore volume of 0.0773 cm^3 g^{-1}.

3.3 Carbon Monoxide Adsorption/Desorption

3.3.1 $NaNi_3(OH)(SIP)_2$

Activation at 513 K in vacuum ($NaNi_3(OH)(SIP)_2$)

Carbon monoxide adsorption and desorption on $NaNi_3(OH)(SIP)_2$ was investigated at pressures up to 20 bar over the temperature range 273–348 K. At 273 K, the adsorption isotherm had a point of inflection corresponding to structural change and the hysteresis was very small (see Figure 2a). At 2 mbar, the hysteresis loop closed (adsorption 0.094 mmol g^{-1} and desorption 0.161 mmol g^{-1}). The isotherm point of inflection gradually became more prominent and the hysteresis increased with increasing temperature up to 303 K, but the desorption isotherm returned to values close to the adsorption isotherm for surface excess values below 1 mmol g^{-1} (see Figures S3a–d). However, the low pressure hysteresis became marked at temperatures ≥ 313 K as shown in the CO adsorption isotherms at 313 K (see Figure 2a and Figures S3e and f). The hysteresis increased with increasing temperature and the CO isotherm at 348 K, shows that approximately half of the CO was retained by the sample under ultra-high vacuum (see Figure 2b). A second sequential isotherm was measured after desorption at 348 K and this is also shown in Figure 2b. This isotherm was Type I in the IUPAC classification scheme[27] and the uptake at 20 bar was the same as the initial isotherm, with the desorption isotherm having some hysteresis, but returning to the starting weight observed following the first isotherm. This indicates that some chemisorption has occurred and a new stable framework was formed on which CO physisorption took place in the second sequential isotherm. The irreversible amount adsorbed was ~ 1.72 mmol g^{-1} and this corresponds to a stoichiometry $NaNi_3(OH)(SIP)_2(CO)_x$ where x = 1.2 (see Figure S4 for confirmation of kinetic equilibration under UHV). The point of inflection in the isotherm suggests that there is framework structural change driven by CO physisorption.

CO Loading Experiments

The effect of CO loading on adsorption hysteresis was investigated in order to establish the relative importance of physisorption and chemisorption in driving the irreversible framework structural change. The CO adsorption/desorption isotherms for $NaNi_3(OH)(SIP)_2$ with loadings up to 0.974 ± 0.015 mmol g^{-1} (5 bar) and 1.43 ± 0.018 mmol g^{-1} (10 bar) at 348 K are shown in Supporting Information (Figure S5a and b, respectively). Both these CO loadings are below the isotherm point of inflection. It is apparent that the isotherms do not show significant adsorption/desorption isotherm hysteresis. The results indicate that at low CO loadings reversible physisorption occurs. An irreversible structural change due to chemisorption only takes place above the point of inflexion in the isotherm as shown in Figures S5c, S5d and 2b for maximum pressures of 15, 17 and 20 bar respectively. The CO 348K isotherm (Figure 2b) above the isotherm point of inflection has both irreversible chemisorption, as shown by the amount remaining after desorption in ultra-high vacuum, and a reversible physisorption contribution, which is the amount desorbed. The physisorbed CO is confirmed by the second sequential isotherm, as shown in Figure 2b. However, for CO adsorption at ≤ 303 K, the isotherms also have points of inflection (see Figures S3a–d), but there is no evidence for chemisorption. This is attributed to the slow kinetics for reaction of CO with the modified framework at lower temperatures.

The isotherm loading experiments at 348 K show that at low pressure, below the point of inflection in the isotherm, reversible non-hysteretic physisorption is observed and the structural change is driven by the enthalpy of adsorption. The surface excess corresponding to the point of inflexion in the CO isotherm for $NaNi_3(OH)(SIP)_2$, increases with increasing temperature. The amount of physisorbed CO corresponding to the point of inflection in the isotherm of $NaNi_3(OH)(SIP)_2$, increases with increasing temperature (see Figure S3). At low temperature (273 K), the point of inflection in the isotherm is at a surface excess ~ 1 mmol g^{-1} (~ 1 CO per 3Ni) whereas it is ~ 2 mmol g^{-1} (~1.5 CO per 3Ni) at 348 K. Below the point of inflection on the isotherm, reversible non-hysteretic physisorption is observed. Above the point of inflection, the sequential isotherm studies demonstrate that the chemisorbed component is irreversible and the physisorbed component is reversible (see Figure 2). Therefore, CO isotherm for $NaNi_3(OH)(SIP)_2$ has both irreversible chemisorption and reversible physisorption components. Carbon dioxide adsorption isotherms on $NaNi_3(OH)(SIP)_2$ after CO adsorption at 348 K were measured in order to determine the change in adsorption characteristics (see Figures S11 and S12). There was a marked change in the CO_2 adsorption

isotherm after CO adsorption and this is consistent with a structural change and a reduction in porosity.

Activation at 403K in Vacuum ($NaNi_3(OH)(SIP)_2(H_2O)_2$)

The activation condition used for the XRD measurements performed at ALS, Berkeley was degassing at 403 K under vacuum and the lower temperature used was a limitation of the equipment. Thermogravimetric analysis shows that only four lattice waters were removed at 403 K under UHV, leaving two coordinated water molecules to form framework $NaNi_3(OH)(SIP)_2(H_2O)_2$. This corresponds to the first plateau in the thermogravimetric profile (see Figure S1). The CO adsorption isotherm for $NaNi_3(OH)(SIP)_2(H_2O)_2$ was measured at 348 K for comparison with the XRD measurements (see Figure S7). The CO adsorption isotherm shows a very small inflection at 15 bar. 1.61 mmol g^{-1} of CO was adsorbed at 20 bar and the desorption branch is hysteretic, but all CO is desorbed under UHV as shown by equilibration in the desorption kinetic profile (see Figure S8). Coordinated water is still present in $NaNi_3(OH)(SIP)_2(H_2O)_2$ and therefore, reactive unsaturated open Ni sites are not available CO.

3.3.2 $NaCo_3(OH)(SIP)_2$

Carbon monoxide adsorption/desorption isotherms for $NaCo_3(OH)(SIP)_2$ at 268 K and 303 K are shown in Figure 3a and S9. It is apparent that at low amounts adsorbed, the isotherm is non-hysteretic, does not have an inflection point in the isotherm, as observed for $NaNi_3(OH)(SIP)_2$ under the same conditions (see Figure 2a), and has lower surface excess at 5 bar pressure (56% of $NaNi_3(OH)(SIP)_2$) (see Figure S9). The isotherm is Type 1 in the IUPAC classification scheme.[30] The carbon monoxide adsorption/desorption isotherm at 348 K and up to 20 bar is shown in Figure 3b. There is a small inflection in the isotherm at 15 bar indicative of structural change. The maximum amount adsorbed is 2.34 mmol g^{-1}, which is 66 wt% of the maximum uptake of $NaNi_3(OH)(SIP)_2$ under the same experimental conditions. The CO adsorption/desorption isotherms show that both $NaCo_3(OH)(SIP)_2$ and $NaNi_3(OH)(SIP)_2$ have points of inflection, but the desorption isotherm for $NaCo_3(OH)(SIP)_2$ was reversible under UHV as shown by desorption kinetic profile in Figure S10. CO_2 adsorption studies showed that the resulting framework had approximately half the uptake of $NaCo_3(OH)(SIP)_2$ (See Figure S11). Therefore, it was concluded that structural change took place after the isotherm point of inflection, but thermally stable CO chemisorption did not occur for $NaCo_3(OH)(SIP)_2$.

3.3.3 Carbon Monoxide Adsorption Thermodynamics

Below the point of inflection in the adsorption isotherms for $NaNi_3(OH)(SIP)_2$ are reversible and only physisorption occurs. The structural change to a new porous framework intermediate structure above the isotherm point of inflection is driven by the enthalpy of physisorption. Both chemisorption and physisorption contribute to the isotherm above the point of inflection. The isosteric enthalpies of adsorption (Q_{st}) and entropies (ΔS) were calculated from the isostere for reversible parts of the isotherms in the temperature ranges 273-343 K for $NaNi_3(OH)(SIP)_2$ and 268–303 K $NaCo_3(OH)(SIP)_2$ (see Figures S17–S20 and Tables S3–S6). The enthalpy of adsorption at zero surface coverage was calculated from low pressure isotherms using a virial equation (Figures S13–S14 and Table S1, for $NaNi_3(OH)(SIP)_2$ and Figures S15–S16 and Table S2 for $NaCo_3(OH)(SIP)_2$).

In the temperature range 303–313 K there is a change in adsorption characteristics for $NaNi_3(OH)(SIP)_2$ from essentially hysteretic adsorption reversible under UHV at 303 K to hysteretic and irreversible adsorption under UHV due to chemisorption occurring above the point of inflection in the isotherm at 313 K. These changes coincide with changes in the graphs of ln(p) versus 1/T which are linear for temperature ranges 273–303 K and 313–343 K. The points of inflection vary from 1.12 mmol g^{-1} at 273 K to 1.18 mmol g^{-1} at 303 K. The Q_{st} in the temperature range 273–303 K was 40.98 ± 2.36 kJ mol^{-1} for surface excess values in the range 0.2 – 1.15 mmol g^{-1} (see Figure 4a). The point of inflection varies from 1.38 mmol g^{-1} at 313 K to 2.05 mmol g^{-1} at 343 K. The Q_{st} in the temperature range 313–343 K was 32.64 ± 1.02 kJ mol^{-1} for surface excess values in the range 0.2 – 1.4 mmol g^{-1}. Therefore, Q_{st} is slightly lower for the temperature range 313–343 K than for 273–303 K. CO isotherms were reversible for temperatures $\leq$ 303 K whereas for temperatures $\geq$ 313 K, substantial non-reversible hysteresis indicative of chemisorption was observed. However, despite the hysteretic characteristics of the adsorption above the point of inflection for temperatures $\geq$ 313 K, at high uptakes, the graphs of ln(p) versus 1/T were linear within experimental error and also over the whole temperature range (273–343 K). Therefore, while there is a clear phenomenological correlation, there are a number of process (structural change, physisorption and chemisorption) taking place simultaneously and hence the interpretation and meaning of Q_{st} determined in this uptake region is unclear. Structural change provides reactive sites for chemisorption of CO. This chemisorbed CO is only released from the framework at 500 K, as definitively shown by in-situ temperature programmed desorption mass spectrometry studies under helium (*vide infra*).

The enthalpy of adsorption at zero surface coverage is a fundamental measure of the CO interaction with the adsorbent and was determined using a virial equation to calculate $\ln(K_H)$ where K_H is the Henry's law constant(Figures S13 and S15). The enthalpy of adsorption at zero surface coverage for CO adsorption on $NaNi_3(OH)(SIP)_2$ was 35.09 ± 0.51 kJ mol^{-1} (See Figure S14) and for $NaCo_3(OH)(SIP)_2$ was 26.6 ± 0.4 kJ mol^{-1}(See Figure S16). The Q_{st} did not vary significantly with increasing uptake (0–0.85 mmol g^{-1}) for $NaCo_3(OH)(SIP)_2$ as shown in Figure 4b. The entropy vs surface excess amount graphs CO adsorption on $NaNi_3(OH)(SIP)_2$ are shown in Figure S21.

3.4 Nitrogen Adsorption at 348 K and Carbon Monoxide/ Nitrogen Selectivity

Nitrogen adsorption on $NaNi_3(OH)(SIP)_2$ and $NaCo_3(OH)(SIP)_2$ at 348 K both gave Type I isotherms in the IUPAC Classification Scheme (see Figure S22). The CO/ N_2 selectivity in the physisorption low pressure region (up to 10 bar) of the CO isotherm was calculated using Ideal Adsorbed Solution Theory (IAST)[31], for a 50:50 gas phase mixture, using CO and N_2 pure component surface excess isotherms at 348 K, as shown in supporting information (Figure S23). The selectivity for CO/N_2 50:50 mixture adsorption on $NaNi_3(OH)(SIP)_2$ increases as the pressure increases from 2.6 at 1 bar to 2.85 at 10.0 bar and for $NaCo_3(OH)(SIP)_2$ was 1.74–1.81 for 0.25–11 bar (see Figure S24). Desolvated Ni_2(dobdc), where dobdc(4-) = 2,5-dioxido-1,4-benzenedicarboxylate, has unsaturated Ni sites and reversible non-hysteretic CO adsorption with higher CO Q_{st} and CO/N_2 selectivity compared with $NaNi_3(OH)(SIP)_2$.[18] The IAST calculations are limited by the maximum spreading pressure determined for nitrogen, the weakest adsorbed component.[32] Therefore, selectivity calculations do not include the CO isotherm region above the point of inflection for $NaNi_3(OH)(SIP)_2$.

3.5 In-Situ Temperature Programmed Desorption (TPD) Studies

3.5.1 TPD of $NaNi_3(OH)(SIP)$ under Ultra-High Vacuum at 1K min^{-1}after CO Sequential Isotherm at 348 K and up to 20 bar

The TPD under UHV after the sequential isotherm experiment was carried out at 1K min^{-1} under UHV (see Figure S25). The weight loss started at ~ 400 K and a stable baseline was obtained after ~100 mins at the maximum temperature used (493 K). The results gave an excellent mass balance with 4.8 wt % desorbed compared with the mass retained of 4.9 wt%. It is evident that virtually all chemisorbed CO can be removed at 493 K under UHV.

3.5.2 Simultaneous Thermogravimetric Analysis combined with Mass Spectrometry under Flowing Helium

Conformation of the composition, thermal stability and mass balance for the desorbed products from the adsorbed phase were investigated by simultaneous in-situ temperature programmed desorption thermogravimetric analysis combined with dynamic mass spectrometry measurements. The isotherm data collection was very time consuming. Therefore, samples were prepared using a fresh sample of $NaNi_3(OH)(SIP)_2$, activated at 513 K and then exposed to 20 bar of CO for 2 weeks. Gravimetric measurements showed that 4.36 wt % was irreversibly adsorbed corresponding to $NaNi_3(OH)(SIP)_2(CO)_{1.09}$. The amount was slightly lower than that obtained from the isotherm measurements. Figure 5 shows the evolved gas peaks and gravimetric data for temperature programmed desorption at 20 K min^{-1} in a helium flow at 1 bar pressure. Mass spectrometer peaks occur at 500 K for m/z 28 (CO), ~600 K for m/z 44 (CO_2) and 615 K for m/z 18(H_2O). The peak at 500 K coincides with the maximum rate of weight loss in the differential thermogravimetric profile (DTG). The CO peak is absent in the corresponding profiles for untreated $NaNi_3(OH)(SIP)_2$ (see Figure S26). This peak is an unequivocal indication that CO chemisorbs reversibly on $NaNi_3(OH)(SIP)_2$ under the experimental conditions used. The presence of a CO_2 desorption peak is also evidence for irreversibly chemisorbed CO since the CO_2 peak is absent in the corresponding profiles for untreated $NaNi_3(OH)(SIP)_2$. However, there are H_2O desorption peaks present in both the CO treated (~615 K) and untreated $NaNi_3(OH)(SIP)_2$ (620 K). These H_2O desorption peaks are attributed to framework decomposition products since $NaNi_3(OH)(SIP)_2$ was activated at a lower temperature (513 K). CO is the only species that desorbed at 500 K in helium and this accounted for 1.69 wt% weight loss giving a stoichiometry $NaNi_3(OH)(SIP)_2(CO)_{0.42}$. The H_2O and CO_2 desorption peaks overlap and the corresponding weight loss peak in the differential thermogravimetric profile was 0.96 wt%. The weight loss (2.65 wt%) loss due to these peaks is less than the total weight gain during adsorption of 4.36 wt% (1.09 CO per formula unit). The remaining weight loss to original starting weight occurs as CO and CO_2 on the leading edge of the thermogravimetric and mass spectrometry peaks corresponding to decomposition of the framework. Temperature programmed heating results in decomposition of the framework with the evolution of CO, CO_2 and SO_2 peaks in the range 700–800 K (See figures S27–S32). The results above show conclusively that CO had reacted with $NaNi_3(OH)(SIP)_2$ to form a new stable framework. CO_2 adsorption studies showed that the resulting CO treated framework had approximately half the uptake of the original untreated $NaNi_3(OH)(SIP)_2$(See Figure S11).

3.6 Structure Characterization

Structural studies were undertaken in order to understand chemisorption in relation to framework structure. Activation of $NaNi_3(OH)(SIP)_2(H_2O)_5 \cdot H_2O$ by heat treatment gave $NaNi_3(OH)(SIP)_2(H_2O)_2$ and $NaNi_3(OH)(SIP)_2$ and both were shown to be crystalline by PXRD (see Figure S2). CO_2 adsorption studies of $NaNi_3(OH)(SIP)_2(H_2O)_2$ and $NaNi_3(OH)(SIP)_2$ showed that total pore volumes increase from 0.0949 to 0.191 $cm^3\ g^{-1}$ on full dehydration. The PXRD profile for $NaNi_3(OH)(SIP)_2$ was indexed in the triclinic space group P-1 with unit cell dimensions and this gave the following: a = 10.8516(5) Å, b = 11.1792(5) Å, c = 12.5215(5) Å, α = 98.575(3)°, β = 106.154(3)°, γ = 67.916(3)°. The comparison of the fit for the Pawley refinement (R_wp = 4.68%) and the experimental data are shown in ESI Figure S2. The crystallographic pore volume was 0.1805 $cm^3\ g^{-1}$ (See ESI, section 1.2) and this value is similar to the total pore volume obtained from CO_2 adsorption studies. CO chemisorption on $NaNi_3(OH)(SIP)_2$ requires degas at 513 K and CO adsorption at 348K and 20 bar with the resulting framework being air/moisture sensitive. The experimental limitations of the facilities available meant that the structure of both the fully dehydrated $NaNi_3(OH)(SIP)_2$ and CO treated samples could not be studied by in-situ single crystal X-ray diffraction. Therefore, only $NaNi_3(OH)(SIP)_2(H_2O)_2$ formed by degas of a single crystal at ~ 400 K could be studied by in-situ techniques. This partially dehydrated structure did not chemisorbed CO and therefore NO was used to probe the availability of unsaturated nickel centres.

3.6.1 The Structure of $NaNi_3(OH)(SIP)_2(H_2O)_5 \cdot H_2O$

$Ni_3Na(C_6H_3(COOH)_2(SO_3))_2(OH)(H_2O)_5 \cdot H_2O$ is a three-dimensional network of composition that crystallises as small free rods into the triclinic space group *P-1* with unit cell dimensions: a = 9.8590(11) Å, b = 11.0355(13) Å, c = 12.5671(14) Å, α = 104.782(2)°, β = 89.974(2)°, γ = 109.954(2)°. The framework consists of Ni_6 clusters that are linked by two structurally distinct μ^7-5-sulfoisophthalate ligands and a 6-coordinate sodium atom. Each Ni_6 cluster is made up of two sets of structurally identical tri-nuclear, octahedral Ni^{II} species consisting of Ni1, Ni2 and Ni3 (see Figure 6). Within the metal cluster, Ni1 is coordinated to Ni2 and Ni3 through a μ^3-hydroxo ligand (O15), which acts as a bridge from which the three Ni octahedra emanate (see Figure 7a). The first μ^7-5-sulfoisopthalate ligand (C1-C8 backbone) bridges two Ni_6 clusters. The first Ni_6 cluster is bound by one of the carboxylate groups and one μ^2-bridging oxygen from its sulfonate group, this leaves the second carboxylate group,

which binds the second Ni_6 cluster (see Figure 7b). The second μ^7-5-sulfoisopthalate ligand (C9-C16 backbone) bridges three Ni_6 clusters, one through each of its sulfonate and carboxylate groups (see Figure 7c). The structure hosts an ill-defined, 'S' shaped channel running down the *z*-axis that hosts crystallised water; when treated as an ellipse with oxygen radii of 1.35 Å, the channel is approximately 3.40 × 0.25 Å (see Figure 8).

3.6.2 The Structure of Partially Dehydrated $NaNi_3(OH)(SIP)_2(H_2O)_2$

Application of a dynamic vacuum of 6 mTorr (8 x 10^{-3} mbar) and heating to 400 K produced a partially dehydrated phase of composition $Ni_3Na(C_6H_3(COOH)_2(SO_3))_2(OH)(H_2O)_2$. The single crystals retained excellent order, and after data collection and structure solution the refinement converged to an R_1 of 4.54 %. Unusually, only the strongly hydrogen bonded O1W and O3W remain, both at full occupancy. Four water molecules have been fully removed – O2W, O4W, O5W and OS. The removal of O4W produced an open metal site on Ni3 as shown in Figure 9. Difference maps were plotted to investigate residual electron density around the Ni3 cluster. It is evident that little or no electron density remains and the water has been removed. These results are consistent with the TGA published previously.[29] The removal of O4W has led to a decrease in the remaining Ni3 – O bond lengths (See CIF files), as nickel has fewer coordinating ligands but the same oxidation state.

3.6.3 Nitric Oxide Loaded $NaNi_3(OH)(SIP)_2(H_2O)_2$

A crystal was exposed to nitric oxide at ~790 Torr to probe whether or not the open metal site is accessible to gases, and was left to equilibrate for one hour at 400 K before data collection. The subsequent refinement converged to an R_1 of 5.89 %. Nitric oxide binds to Ni3 in a bent geometry (see Figure 10). The refined Ni3 – NG bond length is 2.166(16) Å, significantly longer than Ni3 - O4W in the hydrated structure (2.074(4) Å). The oxygen of NO was disordered across two positions, OGA and OGB; their thermal parameters were fixed to 0.08 $Å^2$ and their N-O bond lengths fixed to 1.15 ± 0.02 Å. Their occupancies refined to 26.9 and 10.6 % for OGA and OGB respectively. They are separated by 1.17(7) Å and form a bent geometry with Ni - N - O bonding angles of 119(2) ° for OGA and 130(4) ° for OGB. Nitrogen was fixed at 40 % occupancy to account for the two oxygen positions, and refined with a thermal parameter of 0.023 $Å^2$. When refined freely, the nitrogen occupancy reached 61 % with a thermal parameter of 0.066 $Å^2$, with both oxygen sites totalling 24 % occupancy. A fixed nitrogen occupancy of 40 % was chosen as it reduced its thermal parameter to be in-line with

framework atoms, the oxygen atoms were then allowed to freely refine and their total occupancy was 37.4 (3.1) %, which is within experimental error of the 1:1 nitrogen to oxygen occupancy expected. Nitrogen and both oxygens were refined isotropically. When both oxygen sites were allowed to anisotropically refine, their ellipsoids deviated extensively along the arc formed from nitrogen to both oxygens, indicating a smeared electron density and heavy disorder. This refinement strategy was chosen so as to not over-parameterise and force the model into a predetermined occupancy for the nitric oxide. Modelling of the oxygens as an arc of positions to encompass the rotational freedom of the oxygen, rather than as two distinct positions was investigated. When more oxygen positions were investigated, their occupancies were too low (sub 5%) to behave sensibly and therefore, refinement with only two oxygen sites was used.

3.6.4 Comparison of the Three Crystal Structures and the Importance of Hemilability

Comparison of figures 6, 9 and 10 show the change in coordination for $NaNi_3(OH)(SIP)_2(H_2O)_5 \cdot H_2O$, $NaNi_3(OH)(SIP)_2(H_2O)_2$ and NO loaded $NaNi_3(OH)(SIP)_2(H_2O)_2$ structures. The change in structure Figure 11 A and B show polyhedral and local views of the hydrated structure, parallel to the crystallographic y axis; C and D the same views of the partially dehydrated structure; and E and F the NO loaded structures. Hydrogen bonding between the remaining water molecules in the partially dehydrated structure and the sulfonate groups are shown by dashed lines. The distance between the sodium atom and the oxygen atom of one of the sulfonate groups (this distance is marked by a double-headed red arrow and the numerical label) reduces significantly between the hydrated and partially hydrated state, and is intermediate in the NO loaded structures.

The important feature to note in this set of structures, all of which were solved from single crystal structures, is the hemilability of the sulfonate groups. We define hemilabile MOFs as those where some bonds from the ligands to metals can be broken/remade, allowing facile chemistry to take place, while the framework structure can be held together by the remaining metal-ligand bonds. Mixed carboxylate/sulfonate ligands, such as the sulfoisophthalate used in $NaNi_3(OH)(SIP)_2$ are good examples of MOFs that demonstrate this type of behaviour, where the weaker metal-sulfonate bonds are labile, while the metal-carboxylate bonds are stronger and less liable to break (under mild conditions). In the $NaNi_3(OH)(SIP)_2(H_2O)_5 \cdot H_2O$, $NaNi_3(OH)(SIP)_2(H_2O)_2$ and NO loaded $NaNi_3(OH)(SIP)_2(H_2O)_2$ structures, the sulfonate group changes its orientation as the material is dehydrated; the marked Na-O distance reduces

significantly from 3.237(5) Å to 2.744(4) Å. This is caused by a rotation of the sulfonate group to bring this oxygen much closer to the sodium atom. Once exposed to NO, the calculated Na-O distance increases once more, although since the NO is not fully occupied, the average Na-O distance is measured, which is intermediate between the two extreme values described above. The orientation of the sulfonate group is therefore dependent on whether ligands are coordinated to the exposed nickel sites or not. Prior to the structural change the CO loading studies show reversible non-hysteretic adsorption, which is consistent with physisorption. When CO physisorption reaches a threshold value it induces structural change to form a reactive structure, which reacts with the CO forming a new stable framework. It is proposed that the structural change makes the nickel site more accessible to CO; a prerequisite reactive structure required for the activated chemisorption process to occur.

4. DISCUSSION

Initially, investigations of the adsorption of CO on porous materials concentrated on zeolites and activated carbons. In the case of the latter charge-balancing ions can be exchanged and the effect on the enthalpy of adsorption of gases investigated.[33, 34] The enthalpy of adsorption increases with increasing charge and electric field gradient and ranges from ~25 kJ mol^{-1} for NaY zeolite to ~35- 50 kJ mol^{-1} for M^{2+} exchange zeolite Y where M = Cu^{2+} , Ba^{2+}, Mn^{2+} and Ca^{2+}. The isosteric enthalpy showed a linear correlation with the ν(C=O) and electric field gradient indicating specific interaction with the metal ion. The adsorption of CO on porous carbons gave lower values (~ 20 kJ mol^{-1}) for the isosteric enthalpies of adsorption.[35]

Pirngruber *et al* investigated adsorption and co-adsorption of CO_2/CH_4/CO mixtures for selectivity pressure swing adsorption on MOFs: MIL-100(Cr), MIL-47(V), MIL-140(Zr)-A, Cu-btc (HKUST-1) where btc = benzene tricarboxylate, and MIL-53(Cr).The results were compared with zeolite NaX (13X) and an activated carbon material (AC35). Low pressure CO adsorption isotherms were reported for these materials. The highest adsorbed CO density was observed for zeolite NaX, where there is a strong polarizing interaction of Na^+ with CO. This strong interaction has been observed in other zeolites. Also, in MIL-100(Cr) there is a strong Lewis acid-base interaction for CO, with the enthalpy of adsorption initially ~ 59 kJ mol^{-1}, and with a sharp decrease to 30 kJ mol^{-1} with increasing surface coverage. The CO interaction in Cu-btc (HKUST-1) was significantly weaker with the adsorption enthalpy ~30 kJ mol^{-1}. MIL-140(Zr)-A, AC35, and MIL-47(V) had the lowest enthalpies for CO adsorption. The OH groups in MIL-53(Cr) were only weakly acidic and the enthalpy of adsorption was low. Sato *et al* reported that a nanoporous crystalline material {[Cu(aip)(H_2O)](solvent)$_n$, (where n is the

number of solvent molecules and aip = azidoisophthalate), when activated at 80°C gave Cu(aip), which selectively adsorbed CO in the presence of N_2 through coordination with copper(II) ions and framework structure modification.[19] However, the enthalpy of adsorption of CO adsorption on Cu(aip) was 19 kJ mol^{-1}, [19] which is similar to the value (19.9 kJ mol^{-1}) obtained for adsorption of CO on a carbon molecular sieve.[35, 36] Bloch *et al* investigated [18] CO adsorption on a metal organic framework series M_2(dobdc) (where M = Mg, Mn, Fe, Co, Ni, Zn; dobdc(4-) = 2,5-dioxido-1,4-benzenedicarbox-ylate) and showed that reversible carbon monoxide adsorption occurred, with both high capacities and CO/N_2 selectivities. The Fe, Co, and Ni frameworks had adsorption capacities of up to 0.9 CO per metal cation at 1 bar. The isosteric enthalpies of CO adsorption ranged from 52.7 kJ mol^{-1} at zero surface coverage for Ni_2(dobdc) to 27.2 kJ mol^{-1} for Zn_2(dobdc) with the series order Ni > Co > Fe > Mg > Mn > Zn. The physisorption of CO on Co_2(dobdc) gave an isosteric enthalpy of adsorption of ~ 49 kJ mol^{-1} at zero surface coverage. The M-CO distances were in the order Ni < Co < Fe < Mg < Mn < Zn and ranged from 2.09(2)Å for Ni-C to 2.49(1) Å for Zn-C. The structural and thermodynamic parameters followed the Irving Williams stability order. Isosteric enthalpies of 37-19 kJ mol^{-1} were obtained for CO adsorption on [Cu_2(tqpt)] (where $tqpt^{2-}$ = 6,6,14,14-tetramethyl-6,14-dihydroquinoxalino[2,3-b]phenazinebis-triazolate). The structure with adsorbed CO on [Cu_2(tqpt)] was investigated using PXRD and showed that one CO molecule was weakly coordinated to the Cu(1) and also CO adsorbed in the pores.[20] CO adsorption on MOF Cu^I-MFU-4***l*** at 213 K was also reported.[37] The above literature results are consistent with the rapid CO breakthrough results obtained in dynamic adsorption investigations by Britt *et al* for a series of MOFs.[17]

In this study we report the reversible CO physisorption and thermally stable CO immobilization induced by structural change driven by physisorption on $NaNi_3(OH)(SIP)_2$. The possible reasons for the CO immobilization above the point of inflection in the CO isotherm for $NaNi_3(OH)(SIP)_2$ are 1) CO chemisorption on reactive Ni sites and 2) a structural change leading to trapping of CO in the framework structure. The high temperature conditions used for framework activation and high pressures used for CO immobilization combined with the framework structure having triclinic symmetry limit crystallographic and spectroscopic characterization that can be used. $NaNi_3(OH)(SIP)_2(CO)_x$ is also air sensitive and therefore it was essential that *in situ* characterization methods were used. The following experiments were carried out in order to distinguish between the possible CO immobilization mechanisms by establishing the factors which influence the CO adsorption characteristics for $NaNi_3(OH)(SIP)_2$: 1) sequential CO isotherms; 2) CO_2 isotherm to characterize the porous

structure of the $NaNi_3(OH)(SIP)_2(CO)_x$; 3) studies of the development of isotherm hysteresis as a function of loading; 4) *in-situ* thermogravimetric analysis was carried to show a mass balance and 5) the desorbed species were monitored using simultaneous thermogravimetric analysis combined with mass spectrometry during the heating process to investigate the decomposition of the chemisorbed phase. In the case of CO trapping in the framework only a single CO desorption peak would be expected while both reversible and irreversible chemisorption are possible for CO chemisorption.

In comparison, the isosteric enthalpies for CO adsorption for both $NaNi_3(OH)(SIP)_2$ and $NaCo_3(OH)(SIP)_2$ were lower than the corresponding M_2(dobdc) framework.[18] The isosteric enthalpy of adsorption for $NaCo_3(OH)(SIP)_2$ was virtually constant at ~ 27 kJ mol^{-1} up to a surface excess of 0.8 mmol g^{-1}. The corresponding measurements for $NaNi_3(OH)(SIP)_2$ are in the range 32–49 kJ mol^{-1}, but the interpretation is more complex due to structural change induced by the adsorption process, which is also influenced by temperature.

The CO isotherms for $NaNi_3(OH)(SIP)_2$ revealed that prior to structural change as revealed by the point of inflection, the isotherms are non-hysteretic and reversible at all temperatures studied, which is consistent with physisorption. The most significant difference is that structural change occurs above the point of inflection in the isotherm, which is driven by physisorption, and this results in a reactive framework structure on which CO is immobilized. The CO mass retention on $NaNi_3(OH)(SIP)_2$ on desorption under UHV was 4.9 wt% at 348 K. The desorption isotherm shows the presence of both CO immobilized on the sample and physisorbed CO, which can be desorbed from the sample. The sequential CO isotherm for $NaNi_3(OH)(SIP)_2$ was reversible returning to the original weight after the first irreversible adsorption indicating physisorbed CO after the first isotherm (see Figure 2). This residual weight can be desorbed by heating under ultra-high vacuum to ~500 K (see Figure S25). Subsequent studies involve treatment of $NaNi_3(OH)(SIP)_2$ with CO at 348 K for 2 weeks. Simultaneous *in situ* temperature programmed desorption thermogravimetric and mass spectroscopy under flowing helium for $NaNi_3(OH)(SIP)_2$ after CO adsorption at 20 bar and 348 K showed desorption peaks for CO at 500 K and CO_2 at ~600 K. Both these peaks were not present in the TG-MS of the untreated $NaNi_3(OH)(SIP)_2$ (see Figures 5 and S26). The weight loss corresponding to this TPD CO peak gave a stoichiometry of $NaNi_3(OH)(SIP)_2(CO)_{0.42}$. It is evident that both reversible and irreversible CO immobilization were observed and this is consistent with chemisorption rather than trapping of CO by structural transformation. The structural studies show that the orientation of the sulfonate group is dependent on whether ligands are coordinated to the exposed nickel sites or not. It is apparent that the framework

structure has been maintained by the stronger carboxylate bonds after structural change driven by the enthalpy of adsorption followed by reaction with CO. It is evident that CO chemisorption takes place at 348 K. It is proposed CO reacts with the Ni in the reactive intermediate framework structure with hemilabile sulfonate bond in a similar manner to NO coordination. In the case of $NaCo_3(OH)(SIP)_2$ there is evidence for structural change from isotherm measurements, but not for thermally stable CO chemisorption. This difference is attributed to the lower Q_{st} for $NaCo_3(OH)(SIP)_2$.

5. CONCLUSIONS

$NaNi_3(OH)(SIP)_2(H_2O)_5{\cdot}H_2O$ and $NaCo_3(OH)(SIP)$ $(H_2O)_5{\cdot}H_2O$ are isostructural with hemilabile sulfonate coordination to the metal. The surface chemistry of both these metal organic framework materials includes sodium ions, highly acidic OH groups and unsaturated metal centers, which can interact with CO. The thermal activation of $NaNi_3(OH)(SIP)_2(H_2O)_5{\cdot}H_2O$ was investigated in detail and shows that structural change occurs initially involving partial dehydration to $NaNi_3(OH)(SIP)_2(H_2O)_2$ at 403 K and then full dehydration at ~ 513 K to give $NaNi_3(OH)(SIP)_2$. Both of these materials are crystalline and porous with the activated $NaNi_3(OH)(SIP)_2$ structure having a gas adsorption total pore volume twice that of the crystallographic pore volume for $NaNi_3(OH)(SIP)_2(H_2O)_2$. The adsorption characteristics of isoelectronic CO and N_2, and also NO, on these isostructural metal organic frameworks were investigated. NO coordinated on to the Ni in $NaNi_3(OH)(SIP)_2(H_2O)_2$. At low pressure reversible CO physisorption occurs influenced by synergistic surface chemistry with confinement in pores, to give a CO/N_2 selectivity of 2.4–2.8 for $NaNi_3(OH)(SIP)_2$. The CO uptakes are significantly greater than observed on activated carbons, carbon molecular sieves and zeolites. The isosteric enthalpies of CO adsorption for $NaNi_3(OH)(SIP)_2$ were ~ 40 kJ mol^{-1} (273–303 K), which decreases to ~ 28 kJ mol^{-1} at higher temperatures (313–343 K). CO loading experiments showed that below the point of inflexion the adsorption/desorption isotherms at 348 K were not hysteretic and reversible. However, above the point of inflection, marked hysteresis was observed with retention of CO. Sequential CO adsorption/desorption isotherm studies at 348 K and 20 bar showed that while the first isotherm was irreversible with gravimetric measurements showing that CO was retained under ultra-high vacuum, subsequent CO adsorption/desorption isotherms were reversible. Hence there is the coexistence of physisorbed and chemisorbed carbon monoxide phases at high pressure after the first adsorption/desorption sequence. The point of inflection in the isotherm is indicative of structural change to a framework structure that is reactive towards CO. In-situ temperature

programmed desorption thermogravimetric measurements showed that the mass retained under ultra-high vacuum after the first adsorption/desorption cycle was thermally stable and that the stoichiometry of the product was $NaNi_3(OH)(SIP)_2(CO)_{1.09}$ based on mass desorbed. In-situ temperature programmed desorption experiments showed desorption peaks for CO at 500 K and CO_2 at 590–600 K. Both these peaks were not present in the TG-MS of the untreated $NaNi_3(OH)(SIP)_2$. It is evident that both reversible and irreversible CO chemisorption were observed. The final weight loss occurs as unresolved CO, CO_2 and H_2O on the low temperature side of the framework decomposition peaks in the TG-MS. It is apparent that the framework structure has been maintained by the stronger carboxylate bonds after reaction with CO. Hence, there is structural change driven by physisorption that provides a reactive intermediate structure, which reacts with CO as shown by transition from non-hysteretic to hysteretic CO adsorption isotherms. As far as we are aware, this is the first observation of chemisorption and immobilization of CO on a metal organic framework. However, CO does not chemisorb on $NaCo_3(OH)(SIP)_2$ under the conditions studied, but there is a point of inflection in the isotherm. It is proposed that the hemilabile sulfonate bond in $NaNi_3(OH)(SIP)_2$ is switchable facilitating structural change to a reactive framework intermediate, which chemisorbs CO forming a new porous MOF with high thermal stability under ultra-high vacuum.

■ ASSOCIATED CONTENT

Supporting Information Available

Powder X-ray crystallography and single crystal structure information are given in section S1. The thermogravimetric analysis and thermogravimetric analysis couple with mass spectrometry shown in sections S1, S8–S9, respectively. The gas adsorption data are included in sections S2–S6 and include gas adsorption isotherms, isosteric adsorption enthalpy calculations, and kinetic profiles. Ideal adsorption solution theory for CO/N2 selectivity are given in section S7. Scanning electron micrographs are shown in section S10. This material is available free of charge via the Internet at http://pubs.acs.org.

■ ACKNOWLEGMENTS

The authors gratefully acknowledge financial support from 'Hemilabile and Switchable Metal Organic Frameworks' EPSRC award EP/K005499/1 and for access to the Advanced Light Source (ALS), Berkeley, California, US. CCDC 1553050-1553053 and 1553467 contain the supplementary crystallographic data for this paper. These data can be obtained free of charge from The Cambridge Crystallographic Data Centre via summary.ccdc.cam.ac.uk/structure-summary

■ AUTHOR INFORMATION

Corresponding Author E-mail: mark.thomas@ncl.ac.uk

■ Notes

The authors declare no competing financial interest.

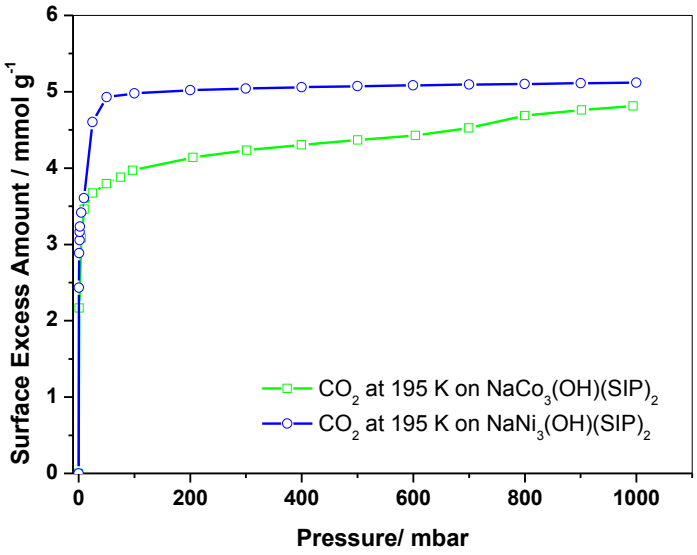

Figure 1. CO_2 adsorption isotherms for $NaCo_3(OH)(SIP)_2$ and $NaNi_3(OH)(SIP)_2$ at 195 K, degassed at 448K and 513K, respectively.

a)

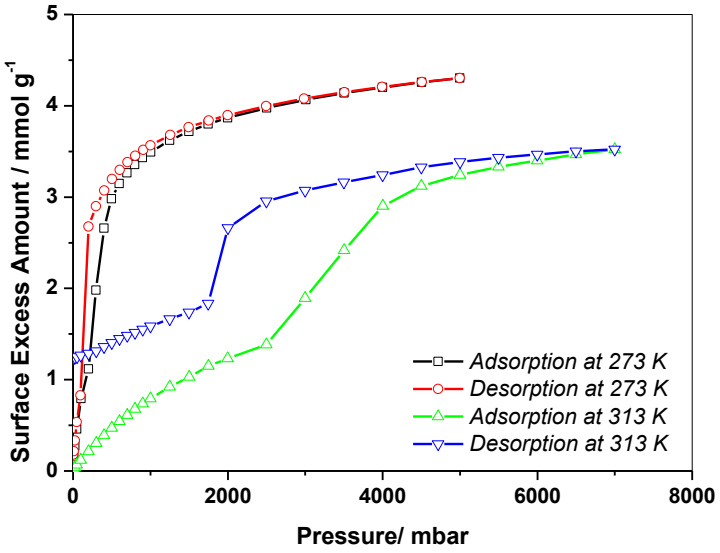

b)

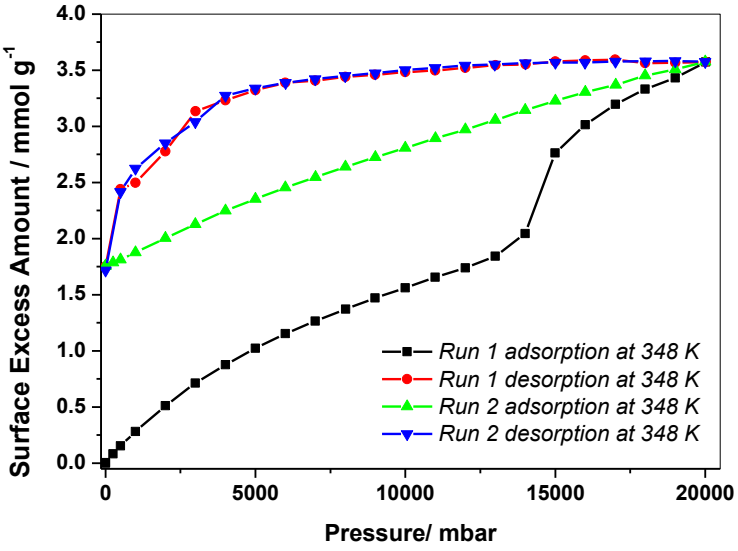

Figure 2. CO adsorption/desorption isotherms for $NaNi_3(OH)(SIP)_2$ degassed at 513 K a) 273 and 313 K b) initial CO adsorption/ desorption on $NaNi_3(OH)(SIP)_2$ at 348 K followed by sequential CO isotherm at 348 K

a)

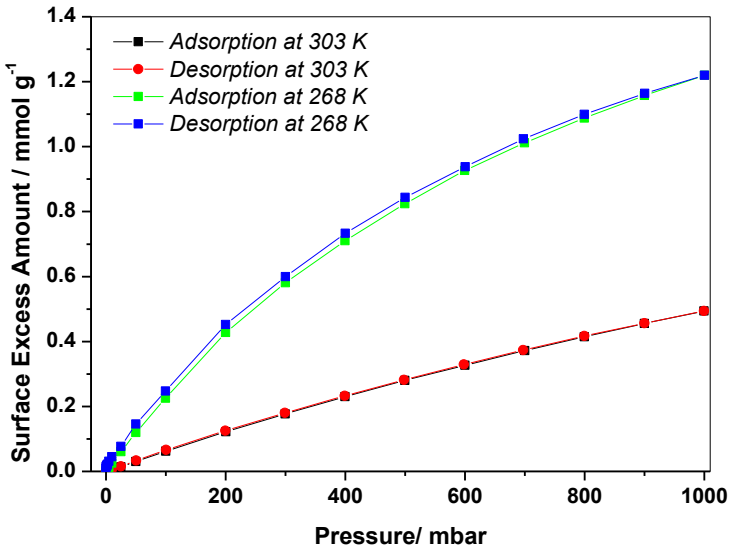

b)

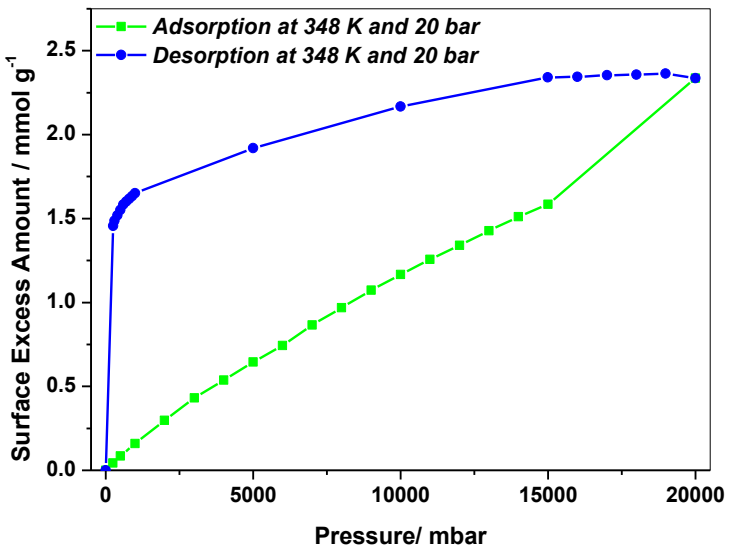

Figure 3. CO adsorption/ desorption isotherms for $NaCo_3(OH)(SIP)_2$ after degas at 448 K at a) 268 K and 303 K and b) 348 K and up to 20 bar

a)

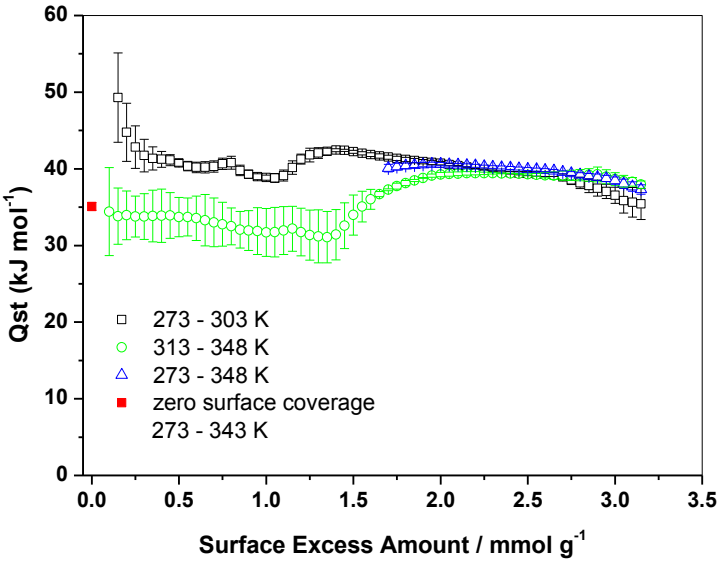

b)

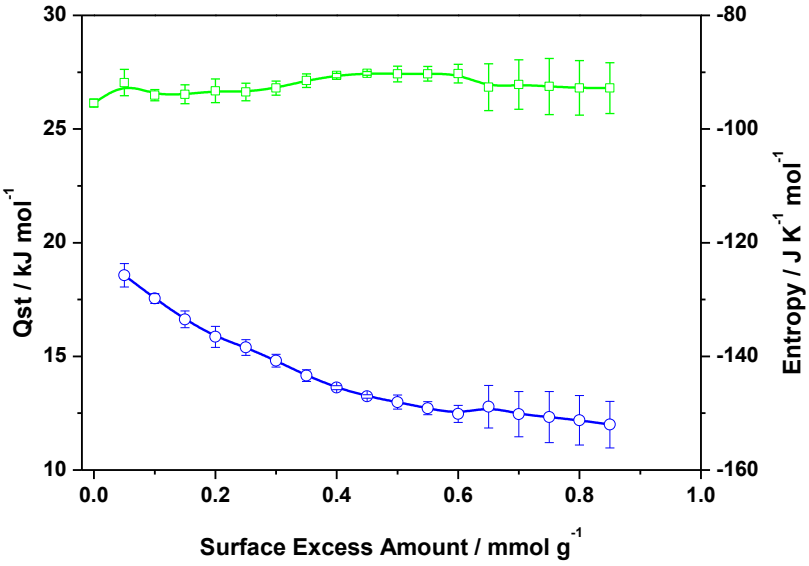

Figure 4. a) Q_{st} (kJ mol^{-1}) versus surface excess (mmol g^{-1}) for CO adsorption on $NaNi_3(OH)(SIP)_2$ over the temperature ranges 273 – 303 K, 313 – 348 K and 273 – 348 K b) Q_{st} and ΔS vs. surface excess (mmol g^{-1}) for CO adsorption on $NaCo_3(OH)(SIP)_2$ over the temperature range 268 – 303 K

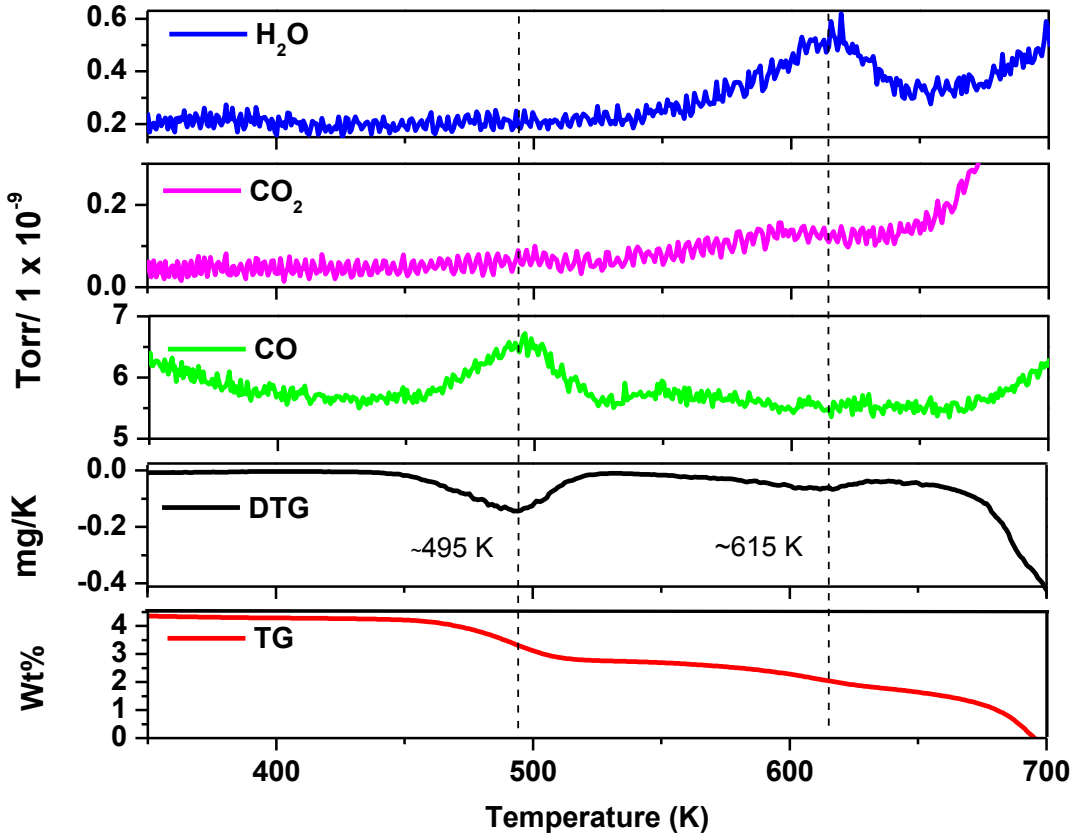

Figure 5: Temperature programmed thermogravimetric, differential thermogravimetric and gas evolution profiles from dynamic sampling mass spectrometry (DSMS) for $NaNi_3(OH)(SIP)_2$ after exposure to CO at 348 K at 20 bar for 2 weeks under dry helium (flow rate 50 cm^3 min^{-1}) for CO, H_2O and CO_2

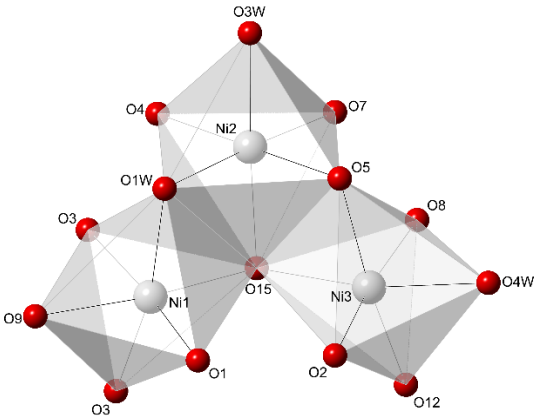

Figure 6: Local structure of $NaNi_3(OH)(SIP)_2(H_2O)_5 \cdot H_2O$ showing all framework waters; a Ni_3 unit when fully hydrated Ni3 with a Ni3-O4W bond length of 2.074(4) Å

a)

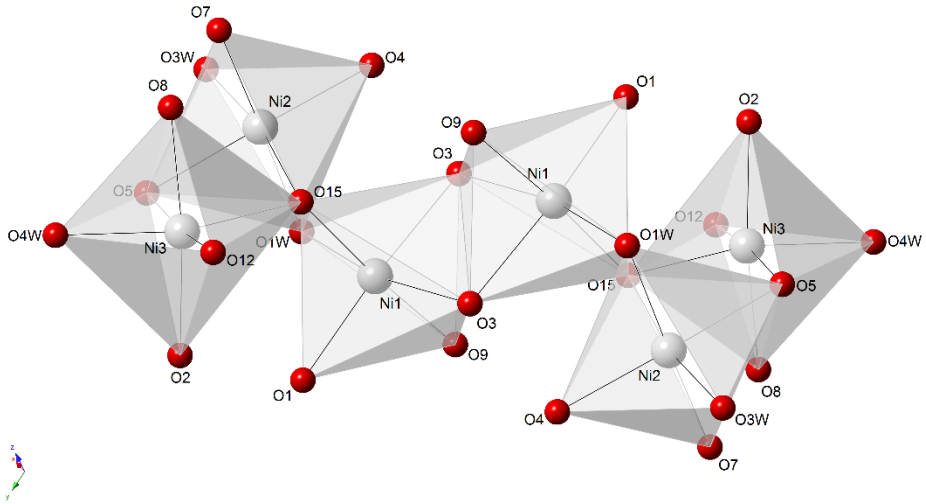

b)

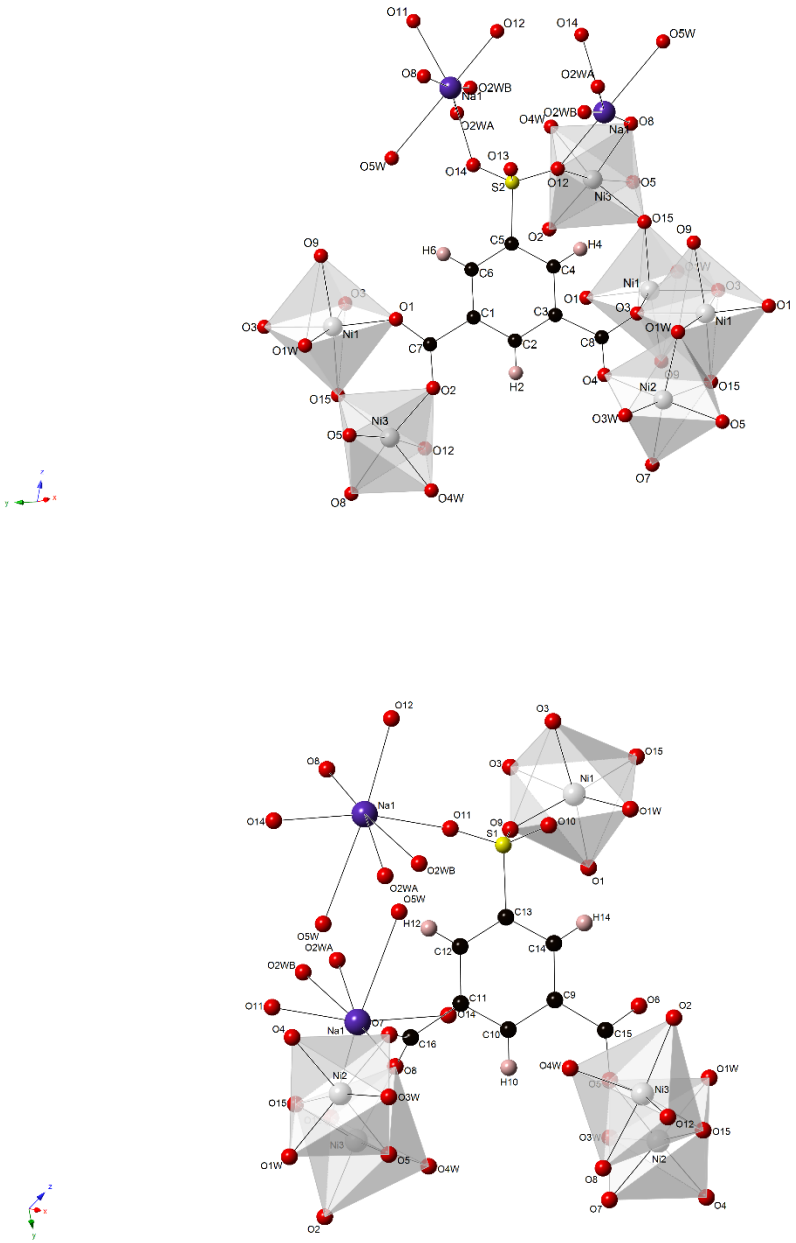

Figure 7. Framework structure of $NaNi_3(OH)(SIP)_2(H_2O)_5{\cdot}H_2O$

a) A Ni_6 cluster made from two sets of symmetrically equivalent Ni_3 motifs. A centre of inversion is at the midpoint between Ni1-Ni1. All oxygens labelled as O#W signify framework bound waters (O1W, O3W and O4W). All other oxygens originate from either carboxylate or sulfonate motifs from either of the two 5-sulfoisophthalate ligands.

b) The first of the two structurally distinct μ^7-5-sulfoisopthalate ligand is shown connecting to two separate but structurally equivalent Ni_6 clusters and 6-coordinate sodium atoms. Nickel

octahedra are shown as silver polyhedra, while sodium, carbon, oxygen, sulfur and hydrogen are shown as purple, black, red, yellow and pink spheres respectively. All atoms that are not linked by one atom or less to the 5-sulfoisophthalate group have been removed for clarity.

c) The second of the two μ^7-5-sulfoisopthalate ligand is shown connecting to three separate but structurally equivalent Ni_6 clusters and two structurally equivalent 6-coordinate sodium atoms. All atoms that are not linked by one atom or less to the 5-sulfoisophthalate group have been removed for clarity. Nickel octahedra are shown as silver polyhedra, while sodium, carbon, oxygen, sulfur and hydrogen are shown as purple, black, red, yellow and pink spheres respectively.

a)

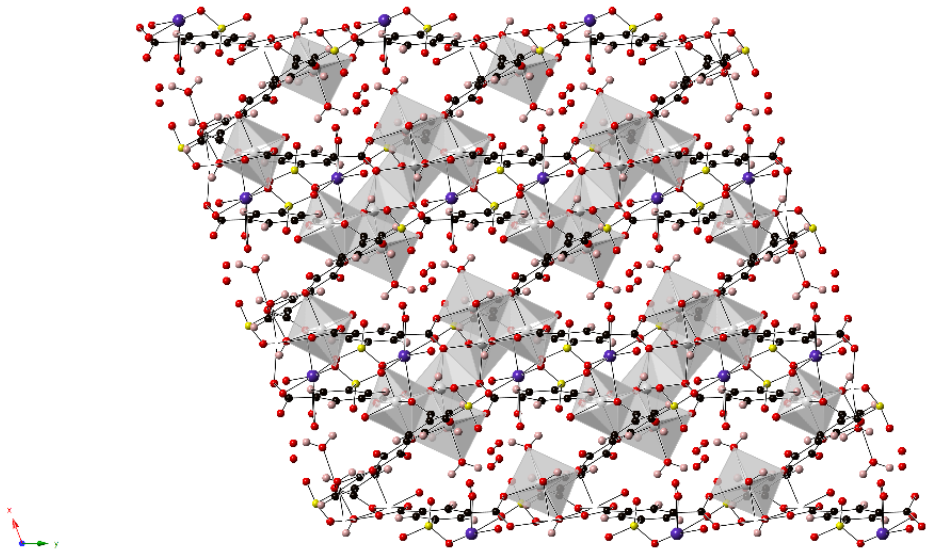

b)

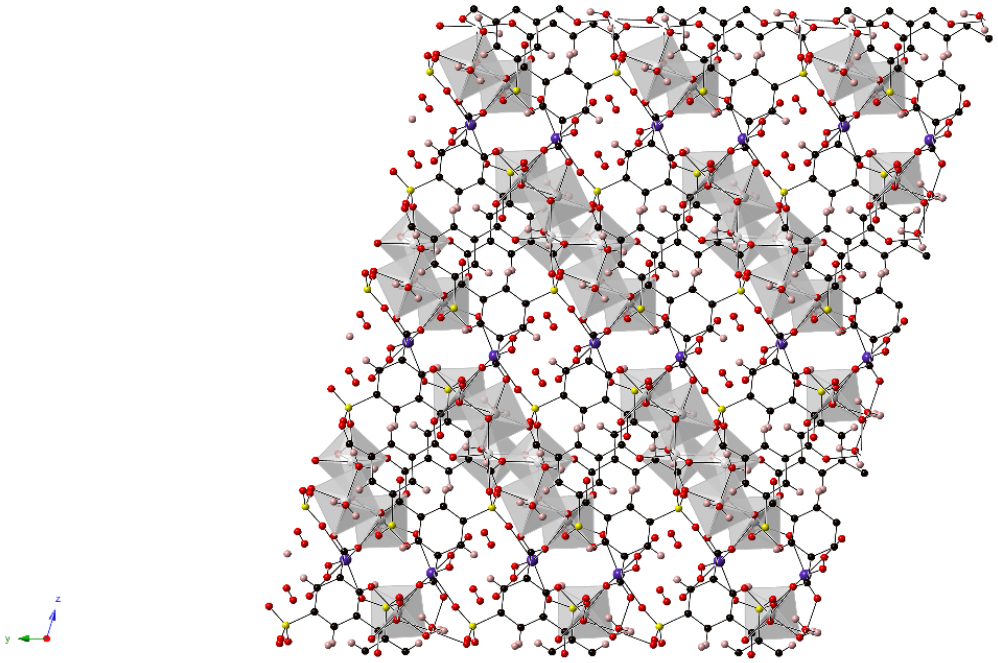

Figure 8: A 3x3x3 supercell as viewed along the *z*-axis (top) and the *x*-axis (bottom), showing the Ni_6 clusters joined by 5-sulfoisophthalate groups and a 6-coordinate sodium. Horizontal S-shaped cavities can be seen containing water of crystallisation. Nickel octahedral are shown as silver polyhedra, while sodium, carbon, oxygen, sulfur and hydrogen are shown as purple, black, red, yellow and pink spheres respectively.

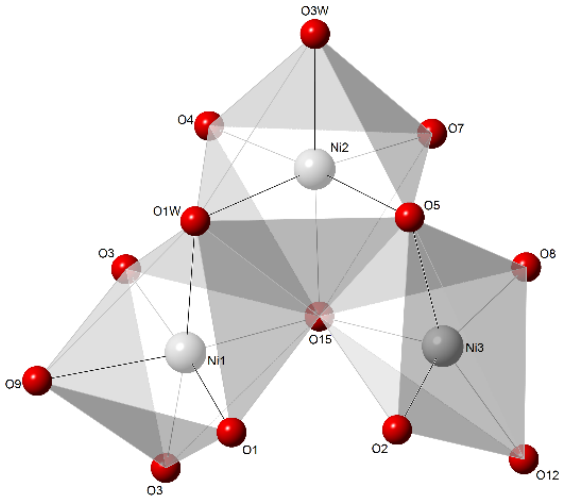

Figure 9. Local structure of $NaNi_3(OH)(SIP)_2(H_2O)_2$, showing the removal of O4W from coordinatively unsaturated Ni3.

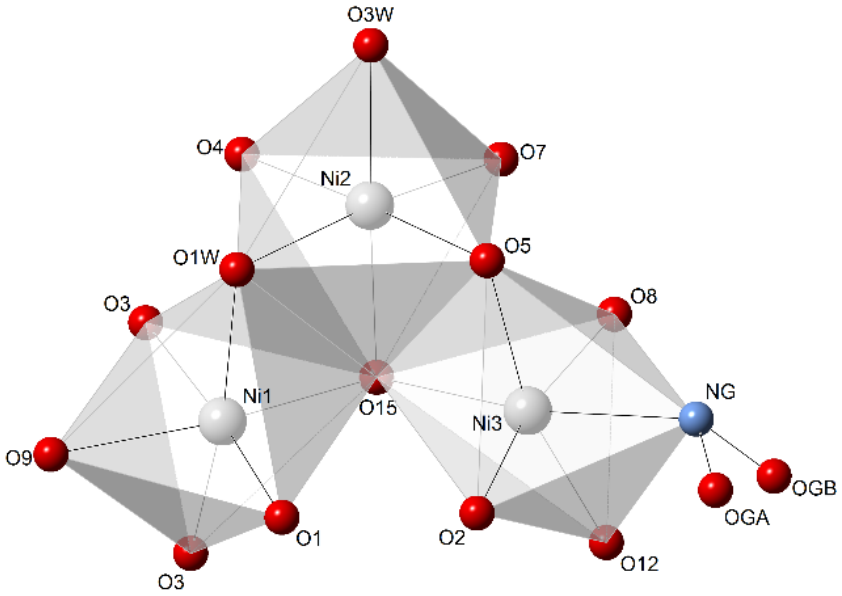

Figure 10. Local structure of $NaNi_3(OH)(SIP)_2(H_2O)_2$, showing nitric oxide bound to Ni3 with a Ni3-N bond length of 2.166(16) Å (bottom), where the oxygen of NO is disordered across two sites OGA and OGB. Nickel polyhedral are shown as silver, oxygen and nitrogen atoms are red and blue spheres respectively.

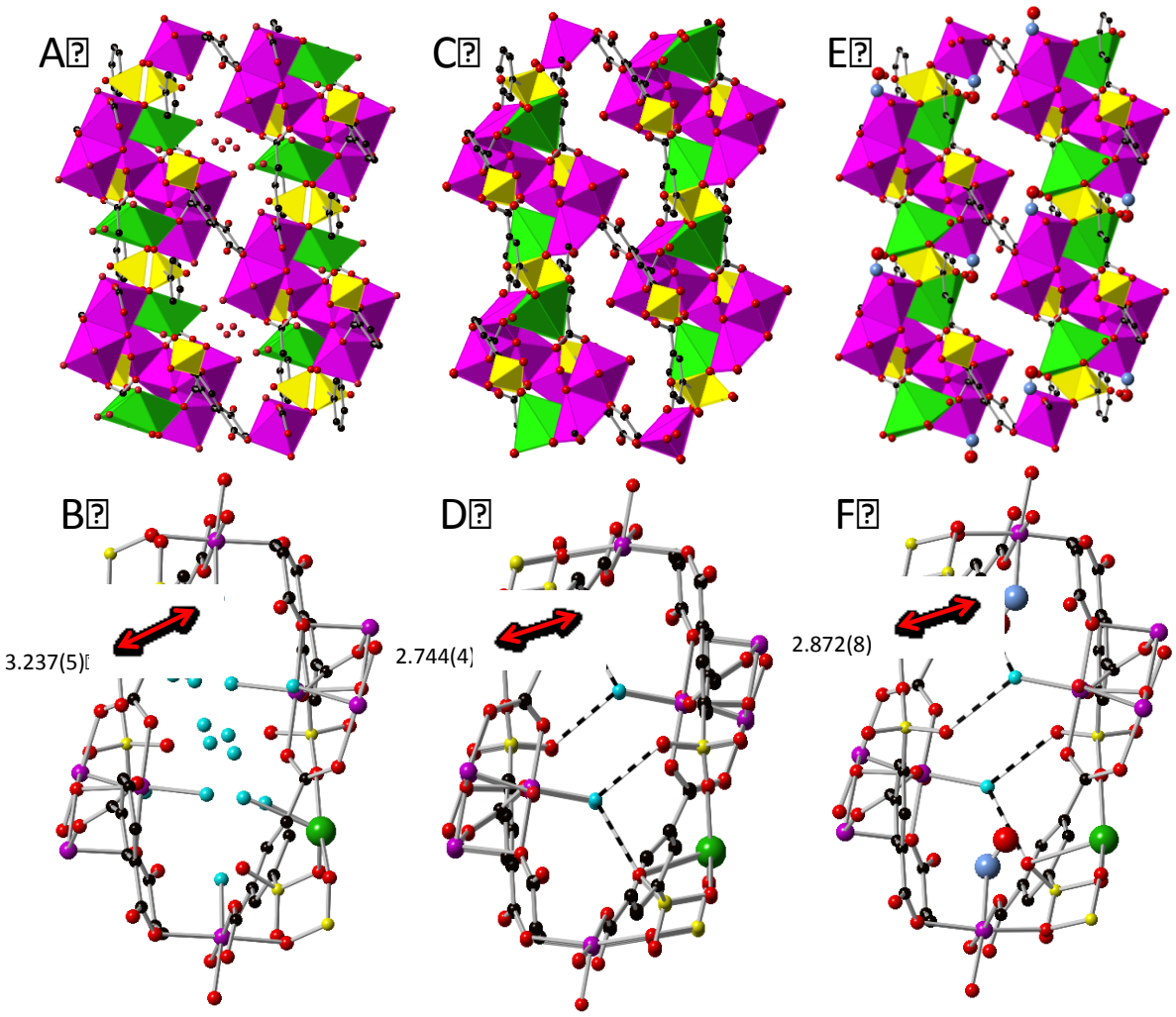

Figure 11. A comparison of the hydrated, partially dehydrated and NO loaded $NaNi_3(OH)(SIP)_2$ crystal structures. The distances marked by the red arrows indicate the distance between the sodium atom and a nearby terminal sulfonate oxygen, showing the hemilabile nature of the SIP ligand as it rotates due to environmental changes (hydrated – A+D, dehydrated – C+D and under nitric oxide – E+F). Colour key: Ni = purple, Na = green, S = yellow, O = red, except for oxygen atoms of water molecules, which are shown as cyan, C = black, N = blue.

REFERENCES

1. Suh, M. P.; Park, H. J.; Prasad, T. K.; Lim, D. W., Hydrogen Storage in Metal-Organic Frameworks. *Chemical Reviews* **2012,** 112, (2), 782-835.
2. Sumida, K.; Rogow, D. L.; Mason, J. A.; McDonald, T. M.; Bloch, E. D.; Herm, Z. R.; Bae, T. H.; Long, J. R., Carbon Dioxide Capture in Metal-Organic Frameworks. *Chemical Reviews* **2012,** 112, (2), 724-781.
3. Liu, J.; Thallapally, P. K.; McGrail, B. P.; Brown, D. R., Progress in adsorption-based CO2 capture by metal-organic frameworks. *Chemical Society Reviews* **2012,** 41, (6), 2308-2322.
4. Chen, B.; Zhao, X.; Putkham, A.; Hong, K.; Lobkovsky, E. B.; Hurtado, E. J.; Fletcher, A. J.; Thomas, K. M., Surface Interactions and Quantum Kinetic Molecular Sieving for H2 and D2 Adsorption on a Mixed-Metal-Organic Framework Material *J. Am. Chem. Soc.* **2008,** 130, (20), 6411-6423.
5. Li, J. R.; Sculley, J.; Zhou, H. C., Metal-Organic Frameworks for Separations. *Chemical Reviews* **2012,** 112, (2), 869-932.
6. Li, J. R.; Kuppler, R. J.; Zhou, H. C., Selective gas adsorption and separation in metal-organic frameworks. *Chemical Society Reviews* **2009,** 38, (5), 1477-1504.
7. Czaja, A. U.; Trukhan, N.; Muller, U., Industrial applications of metal-organic frameworks. *Chemical Society Reviews* **2009,** 38, (5), 1284-1293.
8. Lee, J.; Farha, O. K.; Roberts, J.; Scheidt, K. A.; Nguyen, S. T.; Hupp, J. T., Metal-organic framework materials as catalysts. *Chemical Society Reviews* **2009,** 38, (5), 1450-1459.
9. Yoon, M.; Srirambalaji, R.; Kim, K., Homochiral Metal-Organic Frameworks for Asymmetric Heterogeneous Catalysis. *Chemical Reviews* **2012,** 112, (2), 1196-1231.
10. Horcajada, P.; Chalati, T.; Serre, C.; Gillet, B.; Sebrie, C.; Baati, T.; Eubank, J. F.; Heurtaux, D.; Clayette, P.; Kreuz, C.; Chang, J. S.; Hwang, Y. K.; Marsaud, V.; Bories, P. N.; Cynober, L.; Gil, S.; Ferey, G.; Couvreur, P.; Gref, R., Porous metal-organic-framework nanoscale carriers as a potential platform for drug delivery and imaging. *Nature Materials* **2010,** 9, (2), 172-178.
11. Horcajada, P.; Gref, R.; Baati, T.; Allan, P. K.; Maurin, G.; Couvreur, P.; Ferey, G.; Morris, R. E.; Serre, C., Metal-Organic Frameworks in Biomedicine. *Chemical Reviews* **2012,** 112, (2), 1232-1268.
12. Xiao, B.; Byrne, P. J.; Wheatley, P. S.; Wragg, D. S.; Zhao, X. B.; Fletcher, A. J.; Thomas, K. M.; Peters, L.; Evans, J. S. O.; Warren, J. E.; Zhou, W. Z.; Morris, R. E., Chemically blockable transformation and ultraselective low-pressure gas adsorption in a non-porous metal organic framework. *Nature Chemistry* **2009,** 1, (4), 289-294.
13. Mohideen, M. I. H.; Xiao, B.; Wheatley, P. S.; McKinlay, A. C.; Li, Y.; Slawin, A. M. Z.; Aldous, D. W.; Cessford, N. F.; Duren, T.; Zhao, X.; Gill, R.; Thomas, K. M.; Griffin, J. M.; Ashbrook, S. E.; Morris, R. E., Protecting group and switchable pore-discriminating adsorption properties of a hydrophilicâ€“hydrophobic metalâ€“organic framework. *Nat. Chem.* **2011,** 3, (4), 304-310.
14. Dutta, N. N.; Patil, G. S., DEVELOPMENTS IN CO SEPARATION. *Gas Separation & Purification* **1995,** 9, (4), 277-283.
15. Pirngruber, G. D.; Hamon, L.; Bourrelly, S.; Llewellyn, P. L.; Lenoir, E.; Guillerm, V.; Serre, C.; Devic, T., A Method for Screening the Potential of MOFs as CO2 Adsorbents in Pressure Swing Adsorption Processes. *ChemSusChem* **2012,** 5, (4), 762-776.
16. DeCoste, J. B.; Peterson, G. W., Metal-Organic Frameworks for Air Purification of Toxic Chemicals. *Chemical Reviews* **2014,** 114, (11), 5695-5727.
17. Britt, D.; Tranchemontagne, D.; Yaghi, O. M., Metal-organic frameworks with high capacity and selectivity for harmful gases. *Proceedings of the National Academy of Sciences of the United States of America* **2008,** 105, (33), 11623-11627.
18. Bloch, E. D.; Hudson, M. R.; Mason, J. A.; Chavan, S.; Crocella, V.; Howe, J. D.; Lee, K.; Dzubak, A. L.; Queen, W. L.; Zadrozny, J. M.; Geier, S. J.; Lin, L. C.; Gagliardi, L.; Smit, B.; Neaton, J. B.;

Bordiga, S.; Brown, C. M.; Long, J. R., Reversible CO Binding Enables Tunable CO/H-2 and CO/N-2 Separations in Metal-Organic Frameworks with Exposed Divalent Metal Cations. *Journal of the American Chemical Society* **2014,** 136, (30), 10752-10761.
19. Sato, H.; Kosaka, W.; Matsuda, R.; Hori, A.; Hijikata, Y.; Belosludov, R. V.; Sakaki, S.; Takata, M.; Kitagawa, S., Self-Accelerating CO Sorption in a Soft Nanoporous Crystal. *Science* **2014,** 343, (6167), 167-170.
20. Schmieder, P.; Denysenko, D.; Grzywa, M.; Magdysyuk, O.; Volkmer, D., A structurally flexible triazolate-based metal-organic framework featuring coordinatively unsaturated copper(I) sites. *Dalton Transactions* **2016,** 45, (35), 13853-13862.
21. Xiao, B.; Byrne, P. J.; Wheatley, P. S.; Wragg, D. S.; Zhao, X.; Fletcher, A. J.; Thomas, K. M.; Peters, L.; Evans, J. S. O.; Warren, J. E.; Zhou, W.; Morris, R. E., Chemically blockable transformation and ultraselective low-pressure gas adsorption in a non-porous metal organic framework. *Nature Chemistry* **2009,** 1, (4), 289-294.
22. Mohideen, M. I. H.; Xiao, B.; Wheatley, P. S.; McKinlay, A. C.; Li, Y.; Slawin, A. M. Z.; Aldous, D. W.; Cessford, N. F.; Dueren, T.; Zhao, X.; Gill, R.; Thomas, K. M.; Griffin, J. M.; Ashbrook, S. E.; Morris, R. E., Protecting group and switchable pore-discriminating adsorption properties of a hydrophilic-hydrophobic metal-organic framework. *Nature Chemistry* **2011,** 3, (4), 304-310.
23. Sheldrick, G. M. *SHELXTL, Crystallographic Software Package* 5.1; Bruker Analytical X-ray Systems Inc.: Madison, WI, US: 1998.
24. Dean, J. A.; Lange, N. A., *Lange's Handbook of Chemistry*. McGraw-Hill: 1999.
25. *Lange's Handbook of Chemistry*. 15th ed.; McGraw-Hill: New York, 1999.
26. Jones, J. M.; Harding, A. W.; Brown, S. D.; Thomas, K. M., Detection of reactive intermediate nitrogen and sulphur species in the combustion of carbons that are models for coal chars. *Carbon* **1995,** 33, (6), 833-843.
27. Sing, K. S. W.; Everett, D. H.; Haul, R. A. W.; Moscou, L.; Pierotti, R. A.; Rouquerol, J.; Siemieniewska, T., Reporting physisorption data for gas/solid systems with special reference to the determination of surface area and porosity (Recommendations 1984). *Pure & Appl. Chem.* **1985,** 57, 603-619.
28. *Handbook of Compressed Gases, 3rd Edition Van Nostrand Reinhold, New York1990*. 3rd ed.; Van Nostrand Reinhold: New York, 1990.
29. Kim, D. S.; Forster, P. M.; Le Toquin, R.; Cheetham, A. K., A thermally stable nanoporous nickel 5-sulfoisophthalate; crystal structure and adsorption properties. *Chemical Communications* **2004**, (19), 2148-2149.
30. Atkinson, D.; McLeod, A. I.; Sing, K. S. W., Adsorptive properties of microporous carbons: primary and secondary micropore filling. *Journal de Chimie Physique* **1984,** 81, (11/12), 791-794.
31. Myers, A. L.; Prausnitz, J. M., Thermodynamics of mixed-gas adsorption. *Aiche Journal* **1965,** 11, (1), 121-127.
32. Gao, S.; Morris, C. G.; Lu, Z. Z.; Yan, Y.; Godfrey, H. G. W.; Murray, C.; Tang, C. C.; Thomas, K. M.; Yang, S. H.; Schroder, M., Selective Hysteretic Sorption of Light Hydrocarbons in a Flexible Metal-Organic Framework Material. *Chemistry of Materials* **2016,** 28, (7), 2331-2340.
33. Egerton, T. A.; Stone, F. S., ADSORPTION OF CARBON MONOXIDE BY CALCIUM-EXCHANGED ZEOLITE Y. *Transactions of the Faraday Society* **1970,** 66, (573), 2364-&.
34. Egerton, T. A.; Stone, F. S., ADSORPTION OF CARBON-MONOXIDE BY ZEOLITE Y EXCHANGED WITH DIFFERENT CATIONS. *Journal of the Chemical Society-Faraday Transactions I* **1973,** 69, (1), 22-38.
35. Reid, C. R.; Thomas, K. M., Adsorption of gases on a carbon molecular sieve used for air separation: Linear adsorptives as probes for kinetic selectivity. *Langmuir* **1999,** 15, (9), 3206-3218.
36. Reid, C. R.; Thomas, K. M., Adsorption kinetics and size exclusion properties of probe molecules for the selective porosity in a carbon molecular sieve used for air separation. *Journal of Physical Chemistry B* **2001,** 105, (43), 10619-10629.

37. Denysenko, D.; Grzywa, M.; Jelic, J.; Reuter, K.; Volkmer, D., Scorpionate-Type Coordination in MFU-4l Metal-Organic Frameworks: Small-Molecule Binding and Activation upon the Thermally Activated Formation of Open Metal Sites. *Angewandte Chemie-International Edition* **2014,** 53, (23), 5832-5836.